

## ARTICLE TYPE

Spectro-polarimetric study to constrain accretion-ejection properties of MCG-5-23-16 using *IXPE* and *NuSTAR* observationsSantanu Mondal,<sup>1</sup> Rwitika Chatterjee,<sup>2</sup> Vivek K. Agrawal,<sup>2</sup> and Anuj Nandi<sup>2</sup><sup>1</sup>Indian Institute of Astrophysics, II Block, Koramangala, Bengaluru 560034, India<sup>2</sup>Space Astronomy Group, ISITE Campus, U. R. Rao Satellite Center, ISRO, Bengaluru, 560037, India

Author for correspondence: S. Mondal, Email: santanumondal.work@gmail.com, santanu.mondal@iiap.res.in.

## Abstract

We conducted a study on the X-ray polarization properties of MCG-5-23-16 by analyzing long-term monitoring data from *NuSTAR* jointly with *IXPE* observations in May and November 2022. The re-analysis of *IXPE* data gives model-dependent polarization degree, PD (%) =  $1.55 \pm 0.99$  and  $1.31 \pm 0.95$  in the energy band 2 – 8 keV, agrees with previous studies within error bars. The model-independent analysis of PD poses an upper limit of  $\leq 3.8$  ( $1\sigma$  level) for the same energy band. The observed upper limit of PD, along with broadband spectral analysis (3 – 79 keV), allowed us to derive corona geometry (i.e. length and height) and the accretion disk inclination ( $\sim 33^\circ$ ). Additional *NuSTAR* observations were also analyzed to gain insights into the accretion flow properties of the source and to estimate the expected polarization during those epochs with PD  $\sim 4.3\%$ . The radius and height of the corona exhibited to vary between  $28.2 \pm 3.1$ – $39.8 \pm 4.6 r_s$  and  $14.3 \pm 1.7$ – $21.4 \pm 1.9 r_s$ , with a mass outflow rate from the corona measuring  $0.14 \pm 0.03$ – $0.2 \pm 0.03$  Eddington rate ( $\dot{M}_{\text{Edd}}$ ). The estimated PD values were nearly constant up to a certain radial distance and height of the corona and then decreased for increasing corona geometry. The spectral analysis further provided an estimate for the mass of the central black hole  $\sim 2 \times 10^7 M_\odot$  and the velocity of the outflowing gas  $\sim 0.16$ – $0.19c$ . Our modeling of the disk-corona-outflows and polarization connection can be extended and validated with data from recently launched India's first X-ray Polarimeter Satellite, offering potential applications to other sources.

**Keywords:** accretion disk, galaxies:active, galaxies: Seyfert, polarization, X-rays: individual: MCG-5-23-16

## 1. Introduction

A recent launch of the *Imaging X-ray Polarimetry Explorer* (*IXPE*; Weisskopf et al. 2016) and *X-ray Polarimeter Satellite* (*XPoSat*)<sup>a</sup> Missions have renewed interest in measuring X-ray polarization from diverse astrophysical systems, in particular from accreting black hole (BH) systems of all scales. Accreting matter puffs up at the inner region of the disk, which not only upscatters soft photons through inverse Comptonization (Sunyaev and Titarchuk 1980; Haardt and Maraschi 1993; Chakrabarti and Titarchuk 1995; Done, Gierliński, and Kubota 2007; Mondal and Chakrabarti 2013; Iyer, Nandi, and Mandal 2015, and references therein) but also polarizes the radiation depending on its thermodynamic properties, geometry, and inclination (Connors, Piran, and Stark 1980; Sunyaev and Titarchuk 1985). Therefore, the measurement of polarization angle (PA) and degree (PD) depends on both corona (Compton cloud) properties as well as the photon energy. Additionally, the presence of outflows from the disk can also produce significant polarization due to scattering effects (Begelman and McKee 1983). The dependence of PD and PA on the optical depth and disk inclination was studied using different geometry of the corona in detail (Dovčiak et al. 2008; Li, Narayan, and McClintock 2009; Schnittman and Krolik 2010, and references therein). Therefore, if the corona properties of a system is well constrained, the PD can be estimated or the vice-versa. Hence, the spectro-polarimetric studies using

broadband data may shed more light on the measurement of polarization and the environment of the corona around BHs.

MCG-5-23-16 is a Seyfert 1.9 galaxy (Veron et al. 1980) located at redshift  $z = 0.00849$  (Wegner et al. 2003). The source is relatively bright in X-rays with  $F_{2-10} = 7 - 10 \times 10^{-11}$  erg cm<sup>-2</sup> s<sup>-1</sup> (Mattson and Weaver 2004) and characterized by moderate neutral absorption ( $N_H \sim 10^{22}$  cm<sup>-2</sup>). It has been extensively studied in the X-ray band to estimate corona properties and spectral high-energy cut-off using *INTEGRAL* and *NuSTAR* observations (Beckmann et al. 2008; Molina et al. 2013; Baloković et al. 2015; Zoghbi et al. 2017).

Furthermore, the X-ray spectrum of this source showed the presence of a soft excess and complex Fe K $\alpha$  emission with a broad and asymmetric narrow line features in *ASCA* (Weaver et al. 1997), *BeppoSAX*, *Chandra*, and *XMM-Newton* (Dewangan, Griffiths, and Schurch 2003; Balestra, Bianchi, and Matt 2004; Braitto et al. 2007; Liu, Zoghbi, and Miller 2023) observations. It indicates the presence of two reflectors, one for a narrow core at 6.4 keV and the other for the broad wing, possibly originating closer to the BH. Later, the broad line was explored with *Suzaku* (Reeves et al. 2007) and reported that the inner radius of the disk is  $20 r_s$ , that originated the line, where  $r_s = 2GM_{\text{BH}}/c^2$  is the Schwarzschild radius, with an inclination of  $50^\circ$ . Additionally, an absorption feature at 7.7 keV was unveiled in these data, pointing to the possible presence of ionized iron outflowing at  $\sim 0.1c$ . Recently, Serafinelli et al. 2023 estimated the disk inclination

a. [https://www.isro.gov.in/XPoSat\\_X-Ray\\_Polarimetry\\_Mission.html](https://www.isro.gov.in/XPoSat_X-Ray_Polarimetry_Mission.html)

of  $41^\circ$  from the broad iron line study using *NuSTAR* observations. Marinucci *et al.* 2022 estimated the disk inclination  $48_{-8}^{+12^\circ}$  from broad Fe  $K\alpha$  line profile. Therefore, the estimation of disk inclination angle is not well settled yet. The mass of the central supermassive BH (SMBH) is  $2 \times 10^7 M_\odot$  derived independently from both X-ray variability (Ponti *et al.* 2012) and infrared lines (Onori *et al.* 2017). The spin parameter is 0.856 (Wang *et al.* 2017) estimated using broadband X-ray data and reflection model.

Along with spectral and timing studies, X-ray polarization provides an independent tool to constrain the accretion properties and coronal geometry. It has been reported that the polarization is extremely sensitive to the geometry of the radiation emitting region and the photon field (Schnittman and Krolik 2010; Beheshtipour, Krawczynski, and Malzac 2017; Tamborra *et al.* 2018, and references therein). To constrain the source coronal geometry, MCG-5-23-16 was targeted by two pointings in 2022 with *IXPE*.

The joint analysis of *XMM-Newton*, *NuSTAR*, and *IXPE* observations in May 2022 by Marinucci *et al.* 2022 obtained a 4.7% (at 99% confidence level) upper limit for the polarization degree (PD) in the 2–8 keV energy band and ruled out the slab geometry of the corona. Later, Tagliacozzo *et al.* 2023 analyzed the *IXPE* data from both May and November 2022 epochs in coordination with *NuSTAR* and estimated the PD to be 3.2 % (at 99% confidence level). The authors further compared their observed estimations with Monte Carlo simulations of the expected polarization properties for different geometries of the corona.

Therefore, we see that polarization can be used as a probe to understand the geometry of the corona and accretion–ejection behavior around the central SMBH. The PD and PA have been measured for the source MCG-5-23-16 using radiative transfer–based models only. However, to date, no physically motivated accretion–ejection based models have been directly employed to fit and understand the polarization properties with the corona geometry or accretion flow parameters. In this work, we have re-analyzed the *IXPE* observations to confirm the previous studies jointly with *NuSTAR* data for both epochs (May and November 2022). Further, other data sets available in the *NuSTAR* archive also analyzed to constrain the corona properties and to predict the polarization behavior. Moreover, we have also estimated the mass outflow rate for all epochs, that connect the disk–corona–outflow geometry with polarization from a single framework.

The paper is organized as follows: in §2 we discuss the observation and data reduction procedure. In §3, we describe the spectro–polarimetric data analysis results, and finally, we draw our conclusions in §4.

## 2. Observation and Data Reduction

Over the past decade, MCG-5-23-16 was observed by *NuSTAR* (Harrison *et al.* 2013), spanning from 2012 to 2022. Most recently, the source was observed in May and November 2022 by *IXPE* (Weisskopf *et al.* 2016), launched on 2021 December 9, consisting of three Wolter-I telescopes, with 3 units of

polarization-sensitive imaging X-ray detector units (DUs) at the respective foci. We used all archival data from both observatories for this source and analyzed them. The observation log is given in Table 1.

*IXPE* provides Level-2 data, which we cleaned and calibrated using standard FTTOOLS tasks with the latest calibration files (CALDB 20230526) available in *IXPE* database. A circular region centered at the source of radius  $60''$  (see Tagliacozzo *et al.* 2023, for details) is used for all detectors. A source-free background region of radius  $100''$  is used to produce background subtracted spectra for I, Q, and U Stokes for all three DUs. Additionally, we applied a weighting scheme, STOKES=NEFF (Di Marco *et al.* 2022) in XSELECT to generate the final Stokes spectra in the 2–8 keV energy band.

The *NuSTAR* data were extracted using the standard NUSTARDAS v1.3.1<sup>b</sup> software. We ran a NUPIPELINE task to produce cleaned event lists and NUPRODUCTS along with CALDB version 20231121 to generate the spectra. We used a region of  $25''$  for the source and  $40''$  for the background using ds9 (Joye and Mandel 2003). The data were grouped with a minimum of 30 counts in each bin using *grppha* command. For the analysis of each epoch of observation, we used the data of both *IXPE* and *NuSTAR* in the energy range of 2–8 keV and 3–79 keV. We used XSPEC<sup>c</sup> (Arnaud 1996) version 12.12.0 for spectral analysis.

**Table 1.** Log of observations of MCG-5-23-16. The \* denotes data used for joint spectro-polarimetric analysis.

Obs. Id.	Exp. (ks)	Epoch	Start Date	End Date
<i>IXPE</i>				
01003399	436	I1	2022-05-14	2022-05-31
02003299	160	I2	2022-11-06	2022-11-23
<i>NuSTAR</i>				
60701014002*	84	N1	2022-05-21	2022-05-23
90801630002*	86	N2	2022-11-11	2022-11-12
60001046008	221	N3	2015-03-13	2015-03-18
60001046006	98	N4	2015-02-21	2015-02-23
60001046004	210	N5	2015-02-15	2015-02-20
60001046002	160	N6	2013-06-03	2013-06-07
10002019001	34	N7	2012-07-11	2012-07-11

## 3. Data Analysis and Results

### 3.1 Model-independent *IXPE* Analysis

The processed Level-2 data were used for polarimetric analysis, using IXPEOBSSIM software v30.0.0 (Baldini *et al.* 2022). Source and background events were extracted using XPSELECT task. We obtained the polarization parameters in the entire *IXPE* band of 2–8 keV using the model-independent PCUBE algorithm of the XPBIN task (Kislat *et al.* 2015). To investigate any possible energy dependence of these parameters, we

b. <https://heasarc.gsfc.nasa.gov/docs/nustar/analysis/>

c. <https://heasarc.gsfc.nasa.gov/xanadu/xspec/>

also binned the 2 – 8 keV data into three equal energy bands of 2 keV each and extracted the polarization parameters (refer Chatterjee et al. 2023; Jayasurya, Agrawal, and Chatterjee 2023 for more details).

**Table 2.** Results of model-independent polarimetric analysis

Parameter	2-4 keV	4-6 keV	6-8 keV	2 – 8 keV
Epoch I1				
Q/I (%)	0.44 ± 1.22	-0.28 ± 1.87	0.60 ± 3.70	0.27 ± 1.26
U/I (%)	2.00 ± 1.22	2.54 ± 1.87	-2.20 ± 3.70	1.33 ± 1.26
PD (%)	2.05 ± 1.22	2.55 ± 1.87	2.28 ± 3.70	1.36 ± 1.26
MDP <sub>99</sub> (%)	3.70	5.67	11.21	3.83
Epoch I2				
Q/I (%)	-1.55 ± 1.12	-0.57 ± 1.85	6.25 ± 4.00	-0.15 ± 1.16
U/I (%)	1.08 ± 1.12	-0.96 ± 1.85	4.96 ± 4.00	1.10 ± 1.16
PD (%)	1.89 ± 1.12	1.12 ± 1.85	7.98 ± 4.00	1.11 ± 1.16
MDP <sub>99</sub> (%)	3.39	5.62	12.15	3.50

The results of our model-independent polarimetric analysis for the two epochs are summarized in Table 2. The energy-dependent analysis as well as measurement over the entire energy band yield only upper limits on the PD (below the minimum detectable polarization at the 99% level), and hence the PA is not quoted. The measured PD and PA in 2 – 8 keV for the two epochs (I1 and I2) are shown in Fig. 1 along with the contours. The dashed lines correspond to PCUBE contours with 1 $\sigma$  (blue), 2 $\sigma$  (red), 3 $\sigma$  (green) levels. As it can be observed, the polarization measurements are constrained just at the 1 $\sigma$  level, although lower than the MDP<sub>99</sub> in every energy bin. This also gives the PD upper limit (99% confidence level) of < 3.8% in epoch I1 and < 3.5% in epoch I2. It has been mentioned in (Tagliacozzo et al. 2023) that the model-dependent contours match with PCUBE contours, however, for I2, we obtained a small difference, the possible reason for that is not clear yet. In the next section, we discuss the model-dependent polarization study.

### 3.2 Model-dependent IXPE Analysis

We further analyzed all Stokes spectra for both epochs using a preliminary model, consisting of absorbed CUTOFFPL convolved with a constant polarization POLCONST which reads in XSPEC as CONST\*TBABS\*POLCONST\*CUTOFFPL. All Stokes spectra for all three DUs in the energy band 2 – 8 keV are fitted simultaneously. The abundance in TBABS model is set to `wilms` (Wilms, Allen, and McCray 2000) throughout the analysis.

We have started the fitting by leaving all the spectral and polarimetric parameters to vary freely. We found that the obtained values of PD and PA are highly sensitive to the values of the spectral parameters. Keeping in mind the limited energy band and the spectral sensitivity of IXPE, we turned to simultaneous NuSTAR observations for obtaining robust spectral fits. Moreover, NuSTAR data showed a Fe K line and a small reflection hump, which have also been taken into account during fitting of spectral data.

The above phenomenological CUTOFFPL model fits to the NuSTAR data returned two spectral parameters, cutoff en-

ergy ( $E_{\text{cut}}$ ) and photon index ( $\Gamma$ ). Subsequently, we re-did the IXPE fits by freezing the values of  $E_{\text{cut}}$  and  $\Gamma$  to the best-fit values from NuSTAR. Note that the addition of a Gaussian line and reflection component neither improves the quality of the fit nor affects the value of the polarisation parameters, hence we did not include these two components while fitting the IXPE data. Therefore, it gives a robust estimation of PA and PD. We obtain an acceptable fit for I1 and a good fit for I2 using this model. We determine the PA =  $37.3^\circ \pm 20.1^\circ$  and  $73.2^\circ \pm 23.1^\circ$  for the epochs I1 and I2, and the PD (%) =  $1.55 \pm 0.99$  and  $1.31 \pm 0.95$ . The confidence contours from the model-dependent analysis are shown in Fig. 1. The solid blue, red, and green contours correspond to 1 $\sigma$ , 2 $\sigma$ , and 3 $\sigma$  levels respectively. The model-dependent polarimetric results are summarized in Table 3.

**Table 3.** All Stokes spectra for all three DUs of IXPE are fitted using TBABS\*POLCONST\*CUTOFFPL model. The best-fitted parameters of the model-dependent polarimetric analysis are summarized here. All errors are estimated at the 1 $\sigma$  level.

Parameters	I1	I2
$N_H$ ( $10^{22}\text{cm}^{-2}$ )	3.08 ± 0.03	1.35 ± 0.02
PD (%)	1.55 ± 0.99	1.31 ± 0.95
PA ( $^\circ$ )	37.3 ± 20.1	73.2 ± 23.1
$\Gamma$	1.66	1.64
$E_{\text{cut}}$ (keV)	122.2	124.2
$\chi^2/dof$	1989/1335	1305/1335

### 3.3 IXPE and NuSTAR Analysis

We performed a broadband spectroscopic analysis combining the 2 – 8 keV IXPE spectra and the 3 – 79 keV NuSTAR spectra from May and November 2022. Additionally, we have analyzed all the NuSTAR archival data for the source MCG-5-23-16 covering a decade of observations (see Table 1) to understand the variation of accretion parameters and predict the polarization degree from the model-fitted parameters. The broadband energy range (2 – 79 keV) covered by the spectra of MCG-5-23-16 showed a broad Fe K $\alpha$  line and a Compton hump above 10 keV. A Gaussian component is used at  $\sim 6.3$  keV for the Fe K $\alpha$  line for all observations. Each epoch of observation was first fitted using a simple power-law model, which returned a moderate fit with  $\chi_r^2 \sim 1.29$  (I1+N1) and 1.17 (I2+N2) for the power-law photon index  $\Gamma \sim 1.8 \pm 0.01$ , this is because the model does not take into account the Compton hump above 10 keV. However, it indicates the presence of another component that is contributing to the excess emission, which can either be reflection (Done, Gierliński, and Kubota 2007) or the signature of mass loss from the corona region. Therefore, we further fit the data using an accretion-disk based two-component advective flow (TCAF, Chakrabarti and Titarchuk 1995) model, including a jet component ( $J_{\text{eTCAF}}$ , Mondal and Chakrabarti 2021) to understand the accretion-ejection and polarization behavior of the source. The  $J_{\text{eTCAF}}$  model takes into account the radiation mechanisms at the base of the jet and

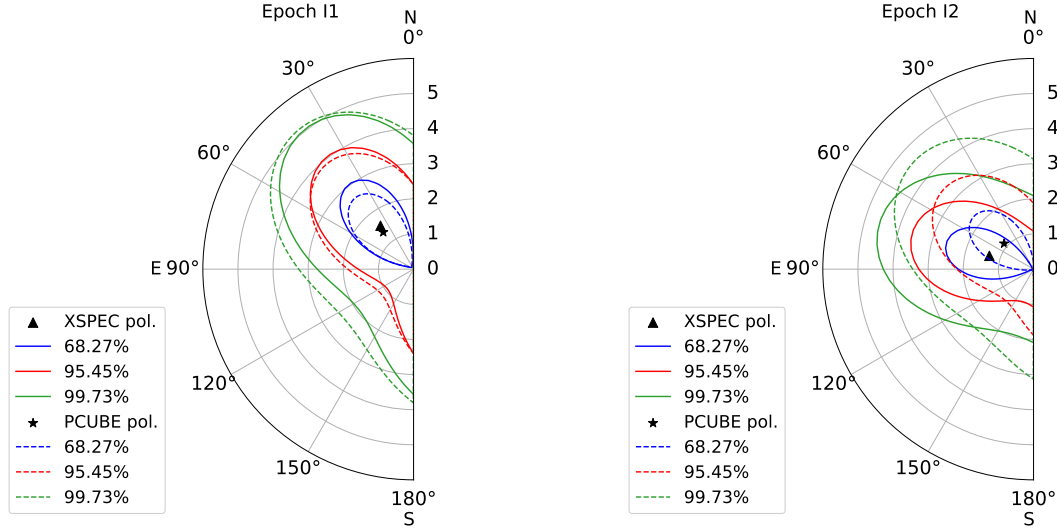


**Figure 1.** XSPEC (solid lines) and PCUBE (dashed lines) contour plots between polarization degree PD and angle PA for May (I1; left) and November (I2; right) epochs in 2022. The blue, red, and green contours denote  $1\sigma$ ,  $2\sigma$ , and  $3\sigma$  confidence levels. See the text for details.

the bulk motion effect by the outflowing jet on the emitted spectra in addition to the Compton scattering of soft disk photons by the hot electron cloud inside the corona. The  $\text{JeTCAF}$  model has six parameters, namely (i) the mass of the BH ( $M_{\text{BH}}$ ) if it is unknown, (ii) the Keplerian disk accretion rate ( $\dot{m}_{\text{d}}$ ), (iii) the sub-Keplerian halo accretion rate ( $\dot{m}_{\text{h}}$ ), (iv) the size of the dynamic corona or the location of the shock ( $X_s$  in  $r_g = 2GM_{\text{BH}}/c^2$  unit), (v) the shock compression ratio ( $R$ ), and (vi) the outflow/jet collimation factor ( $f_{\text{col}}$ ), the ratio of the solid angle subtended by the outflow to the inflow ( $\Theta_o/\Theta_{\text{in}}$ ). The hydrogen column density for Galactic absorption set fixed to  $7.8 \times 10^{20} \text{ cm}^{-2}$  (HI4PI Collaboration et al. 2016; Kalberla et al. 2005) during the fitting. For the host galaxy absorption, we used the ZTBABS model with `wilm` abundance. The full model reads in XSPEC for *IXPE* and *NuSTAR* as `TBABS*ZTBABS(JeTCAF+GAUSS)`.

In Fig. 2, we show the model-fitted spectra of MCG-5-23-16 for the joint *IXPE* and *NuSTAR* observations. The Fe  $K\alpha$  line fitted well with a Gaussian line width of  $\sim 0.3$  keV for all observations and the Compton hump fitted with  $\text{JeTCAF}$  model that takes it into account by the scattering of corona photons by the diverging outflow. The disk mass accretion rate in  $\text{JeTCAF}$  model varied minimally, whereas the halo accretion rate was nearly constant  $\sim 0.4 \dot{M}_{\text{Edd}}$  and the size of the corona changed significantly from  $\sim 28$  to  $40r_s$ . As the mass of the BH is a parameter in this model, one can also estimate the BH mass. The model fit to all the epochs gives nearly a constant mass of the central SMBH  $\sim 2 \times 10^7 M_{\odot}$ , consistent with previous estimations in the literature. For the joint epochs data (I1+N1 and I2+N2) fits, the  $N_{\text{H}}$  for the host galaxy absorption required in ZTBABS model is  $2.0 - 2.2 \times 10^{22} \text{ cm}^{-2}$ , while earlier *NuSTAR* epochs (N3-N7) required  $N_{\text{H}} \sim 1.2 - 1.5 \times 10^{22} \text{ cm}^{-2}$ . The high value of the  $f_{\text{col}}$  parameter implies that the outflow is not well collimated and the rate is high. The estimated outflow solid angle is  $\sim 0.5\pi$ .

All model parameters are summarized in Table 4.

From the  $\text{JeTCAF}$  model fitted parameters, we have estimated different physical quantities to understand the variation of polarization with corona geometry and spectral flux. The height of the corona is basically the height of the shock, as the shock is the boundary layer of the corona. The height of the shock ( $h_{\text{shk}}$ ) is estimated using (Debnath, Chakrabarti, and Mondal 2014),  $h_{\text{shk}} = [\gamma(R-1)X_s^2/R^2]^{1/2}$ , where,  $\gamma$  is the adiabatic index of the flow, which is considered here as  $5/3$ . The estimated  $h_{\text{shk}}$  varies in a range between  $\sim 14 - 21 r_s$ .

The mass outflow rate ( $\dot{m}_{\text{out}}$ ) is derived for an isothermal base of the jet (Chakrabarti 1999), which is given by,

$$\dot{m}_{\text{out}} = \dot{m}_{\text{in}} f_{\text{col}} f_0^{3/2} \frac{R}{4} \exp\left[\frac{3}{2} - f_0\right], \quad (1)$$

where,  $f_0 = \frac{R^2}{R-1}$  and  $\dot{m}_{\text{in}}$  is the total mass inflow rate. The estimated  $\dot{m}_{\text{out}}$  varies between  $0.14 \pm 0.03 - 0.20 \pm 0.03 \dot{M}_{\text{Edd}}$  for this source, which is significant as was reported earlier in the literature (see, Braito et al. 2007). According to this model, as mentioned earlier, both corona and base of the jet behave as a Comptonizing medium. The radiation scattered by the corona or wind may exhibit significant polarization. The unpolarized radiation from the central source scattered by the corona of radius  $X_s$  at height  $h_{\text{shk}}$  above the midplane of the disk will acquire a net fractional polarization (Begelman and McKee 1983),

$$\Pi_{\text{sc}} = \frac{\sin^2 i [1 - 2(h_{\text{shk}}/X_s)^2]}{2[1 + 2(h_{\text{shk}}/X_s)^2] + [1 - 2(h_{\text{shk}}/X_s)^2] \sin^2 i}, \quad (2)$$

where  $i$  is the disk inclination angle. As this model assumes Thomson scattering and negligible Comptonization, thereby, the scattering conserves photon energy. Moreover, the Thomson scattering has no frequency dependence so it would preserve the incident spectrum for any energy bands including

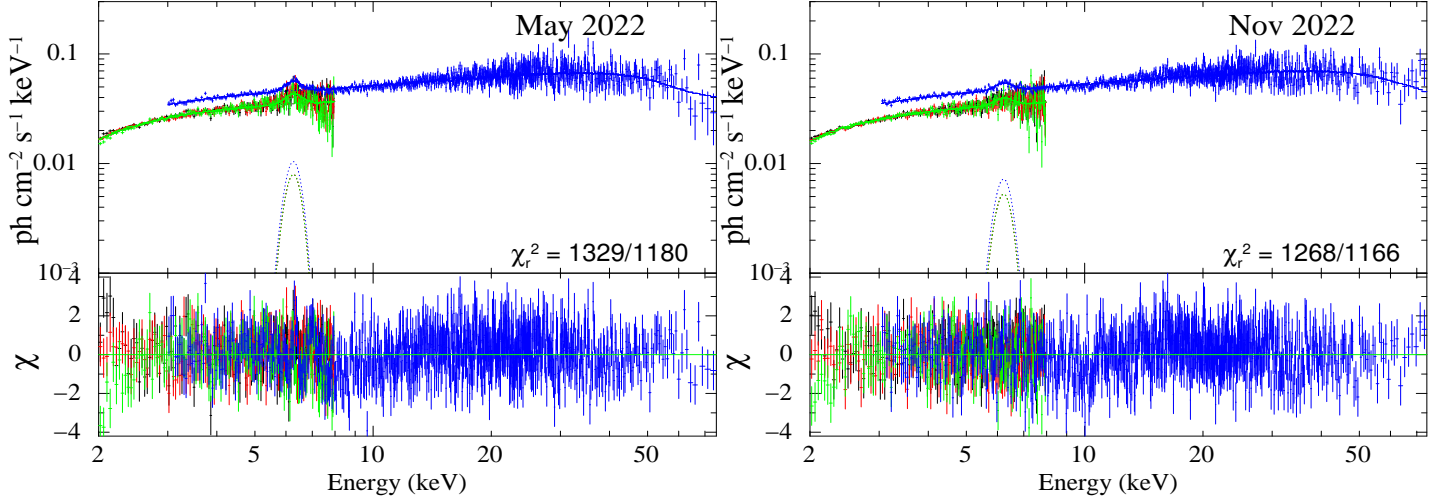


**Figure 2.** Joint spectral modelling of *IXPE* and *NuSTAR* data fitted using *JeTCAF* model in the energy band 2 – 79 keV. The left and right panels are for the epochs (I1+N1) and (I2+N2). The Fe  $K\alpha$  line  $\sim 6.3$  is fitted using *GAUSS* model as shown by dashed lines. The black, red, and green points correspond to *IXPE* data for all three DUs and the blue points correspond to *NuSTAR* data. See the text for details.

**Table 4.** Joint *IXPE* and *NuSTAR* data fitted model parameters are provided in this table. Here,  $M_{\text{BH}}$ ,  $\dot{m}_d$ ,  $\dot{m}_h$ ,  $X_s$ ,  $R$ , and  $f_{\text{col}}$  are the mass of the BH, disk and halo mass accretion rates, location of the shock or size of the corona, the shock compression ratio, and the outflow collimation factor respectively in *JeTCAF* model.  $N_H$  is the hydrogen column density in *ZTBABS* model. All data sets required *GAUSS* model for the Fe  $K\alpha$  line  $\sim 6.3$  keV of width  $\sigma_g$  given in the table.

Model	JeTCAF						ZTBABS	GAUSS	
Epoch	$M_{\text{BH}}$ ( $10^7 M_{\odot}$ )	$\dot{m}_d$ ( $10^{-2} \dot{M}_{\text{Edd}}$ )	$\dot{m}_h$ ( $\dot{M}_{\text{Edd}}$ )	$X_s$ ( $r_s$ )	R	$f_{\text{col}}$	$N_H$ ( $10^{22} \text{ cm}^{-2}$ )	$\sigma_g$ (keV)	$\chi_r^2/dof$
I1+N1	$2.0 \pm 0.3$	$1.3 \pm 0.2$	$0.41 \pm 0.03$	$38.3 \pm 4.4$	$4.91 \pm 0.51$	$0.53 \pm 0.07$	$2.21 \pm 0.25$	$0.30 \pm 0.03$	1329/1180
I2+N2	$2.1 \pm 0.2$	$0.9 \pm 0.1$	$0.40 \pm 0.03$	$39.4 \pm 3.4$	$4.36 \pm 0.23$	$0.49 \pm 0.04$	$2.04 \pm 0.39$	$0.31 \pm 0.04$	1268/1166
N3	$2.1 \pm 0.2$	$1.2 \pm 0.2$	$0.40 \pm 0.02$	$28.2 \pm 3.1$	$5.24 \pm 0.38$	$0.45 \pm 0.04$	$1.37 \pm 0.11$	$0.27 \pm 0.02$	1102/989
N4	$1.9 \pm 0.2$	$1.3 \pm 0.1$	$0.41 \pm 0.03$	$34.9 \pm 3.9$	$5.19 \pm 0.32$	$0.49 \pm 0.05$	$1.22 \pm 0.09$	$0.31 \pm 0.03$	864/768
N5	$2.0 \pm 0.1$	$1.3 \pm 0.1$	$0.41 \pm 0.02$	$29.9 \pm 2.1$	$5.28 \pm 0.42$	$0.47 \pm 0.03$	$1.49 \pm 0.15$	$0.31 \pm 0.02$	1029/928
N6	$2.1 \pm 0.1$	$1.1 \pm 0.1$	$0.41 \pm 0.04$	$39.8 \pm 4.6$	$4.98 \pm 0.37$	$0.54 \pm 0.03$	$1.27 \pm 0.07$	$0.35 \pm 0.03$	983/930
N7	$2.0 \pm 0.1$	$1.3 \pm 0.1$	$0.42 \pm 0.02$	$37.9 \pm 2.8$	$5.06 \pm 0.30$	$0.53 \pm 0.04$	$1.14 \pm 0.15$	$0.27 \pm 0.02$	609/570

*IXPE* coverage. Therefore, for a given or well-estimated corona properties and disk inclination, one can estimate PD or vice-versa using Eq. 2. As the disk inclination is not well constrained in the literature, we have estimated it from the observed upper limit of the PD in Tagliacozzo *et al.* 2023 and the broadband spectroscopic data fitted  $\text{J}e\text{TCAF}$  model parameters. Our estimated  $i$  ranges between  $31^\circ - 35^\circ$  during I2 and I1 epochs. These estimations are further applied to predict the expected PD for other epochs during *NuSTAR* observation. All estimated parameters are given in Table 5. The spectral flux given in the table is calculated using `flux_err` command in *XSPEC* for the energy band 2 – 79 keV.

**Table 5.** Estimated and observed polarization and corona properties of MCG-5-23-16. The 3 – 79 keV band flux is in units of  $10^{-10}$  erg  $\text{cm}^{-2}$   $\text{s}^{-1}$ . Here,  $^{a,b}$  denotes the references to Marinucci *et al.* 2022 and Tagliacozzo *et al.* 2023. In the first two rows,  $^c$  denotes the estimation of  $i$  from the observed upper limit of PD, while the expected PDs in column 5 are calculated for  $i = 33^\circ$ .

Epoch	$\dot{m}_{\text{out}}$ ( $\dot{M}_{\text{Edd}}$ )	$h_{\text{shk}}$ ( $r_s$ )	$F_{3-79\text{keV}}$	PD(%)		$i$ (deg)
				Model	Obs. $^{a,b}$	
I1+N1	$0.19 \pm 0.04$	$19.9 \pm 2.5$	$2.75 \pm 0.02$	4.2	$\leq 4.7$	$35^c$
I2+N2	$0.20 \pm 0.03$	$21.4 \pm 1.9$	$2.84 \pm 0.02$	3.7	$\leq 3.3$	$31^c$
N3	$0.14 \pm 0.03$	$14.3 \pm 1.7$	$2.66 \pm 0.03$	4.5	-	33
N4	$0.16 \pm 0.02$	$17.8 \pm 2.1$	$2.53 \pm 0.01$	4.5	-	33
N5	$0.15 \pm 0.02$	$15.1 \pm 1.2$	$2.30 \pm 0.02$	4.6	-	33
N6	$0.19 \pm 0.03$	$20.6 \pm 2.5$	$3.09 \pm 0.02$	4.3	-	33
N7	$0.19 \pm 0.02$	$19.5 \pm 1.6$	$2.87 \pm 0.02$	4.4	-	33

The left panel of Fig. 3 shows the variation of PD with the radial distance of the corona. The red circles are the PD values estimated using the model fitted  $h_{\text{shk}}$  and  $X_s$  parameters for a given  $i = 33^\circ$ , which is the average of disk inclination angles estimated from the upper limit of the observed PD values reported in Tagliacozzo *et al.* 2023. For a corona of  $< 35 r_s$ , the PD was nearly constant and it decreased when the corona size increased. A similar profile has been observed (middle panel of Fig. 3) for the height of the corona, which is quite expected as a bigger corona indicates a hotter electron cloud and more puffed up in the vertical direction. Our estimated PD variation with corona geometry is in accord with the simulation results performed by Schnittman and Krolik 2010 for a spherical geometry of the corona. The right panel of Fig. 3 shows the PD variation with estimated spectral flux, which shows a negative correlation as well.

#### 4. Discussions

In this work, we have performed the spectro-polarimetric analysis of the Seyfert galaxy MCG-5-23-16 to understand the polarization properties and the X-ray emitting corona using two epochs of data from *IXPE* and a decade of observations from *NuSTAR*. Our model-independent analysis poses the PD with an upper limit of  $\leq 3.8\%$ , while the model-dependent estimates give PD  $1.55 \pm 0.99\%$  and  $1.31 \pm 0.95\%$  for the epochs I1 and I2, while the PA values are  $37.3^\circ \pm 20.1^\circ$  and  $73.2^\circ \pm 23.1^\circ$ , which are in accord with the previous studies within error bar (Marinucci *et al.* 2022; Tagliacozzo *et al.* 2023).

The joint *IXPE* and *NuSTAR* broadband spectroscopic data fitting gives also the estimate of disk mass accretion rate to the central SMBH which is  $\leq 0.013 \dot{M}_{\text{Edd}}$ , while the halo accretion rate is  $\leq 0.4 \dot{M}_{\text{Edd}}$ . The location of the shock changed from 28 to 40  $r_s$  and the shock compression ratio varied between 4.4 – 5.3. Relatively high values of jet/outflow collimation factor indicate that the outflow is not well-collimated. The previous studies reported that the source showed significant mass outflow, here we estimated the mass outflow rate  $\sim 0.14 - 0.20 \dot{M}_{\text{Edd}}$  from the spectral model fitted parameters. Since mass outflow carries thermal energy from the hot corona, its geometry changes (Chakrabarti 1999; Mondal, Chakrabarti, and Debnath 2014). Therefore, the final best-fit corona geometry which is used to estimate the expected PD has the effect of mass outflows. Hence, studying polarization using the disk-corona-outflows model is crucial to get a consistent picture of a system, which has been done in this work.

The estimation of disk inclination for this source is not well constrained to date. As the scattering of photons inside the Comptonizing corona or outflow can induce significant polarization, we use it to further estimate the disk inclination for a given corona geometry, mainly with its radial distance and height. Using the polarization information we have estimated the upper limit of the disk inclination  $\sim 35^\circ$  for the highest measured polarization in May 2022 and  $\sim 31^\circ$  in November 2022. After taking an average of these two estimates, we further use it to determine the expected polarization during the epochs N3–N7. The estimated PD decreases with increasing the corona geometry at different epochs (see Fig. 3). Our study not only relates the polarization with the accretion flow properties but also can predict expected polarization which can be further applied and verified using *XPoSat* observations of this source – which includes a polarimeter (POLIX: 8 – 30 keV) and spectrometer (XSPECT: 0.8 – 15 keV) can shed further light on the accretion properties of this source and verify the model-predicted results. POLIX, having an energy band complementary to that of *IXPE*, can help constrain the polarimetric properties of this source over a wider energy range. Preliminary analysis suggests that POLIX observations can constrain the PD of this source in  $\sim 1$  Ms, whereas the spectral properties can be constrained by XSPECT in  $\sim 200$  ks. These conservative estimates show that simultaneous observation of this source by these two instruments can further reveal its properties and dynamics around the central object. Additionally, current model prescription can also be applied to other Seyfert galaxies to study their X-ray polarization in connection with the accretion–ejection properties, where polarization could be due to reflection (NGC 4151; Gianolli *et al.* 2023) or outflowing jet (IC 4329A; Ingram *et al.* 2023; Pal *et al.* 2023), which will be addressed in future.

#### Acknowledgement

SM thanks Keith A. Arnaud for helping during the data analysis. RC, VKA, and AN thank GH, SAG, DD, PDMSA, and the Director, URSC for continuous support to carry out the

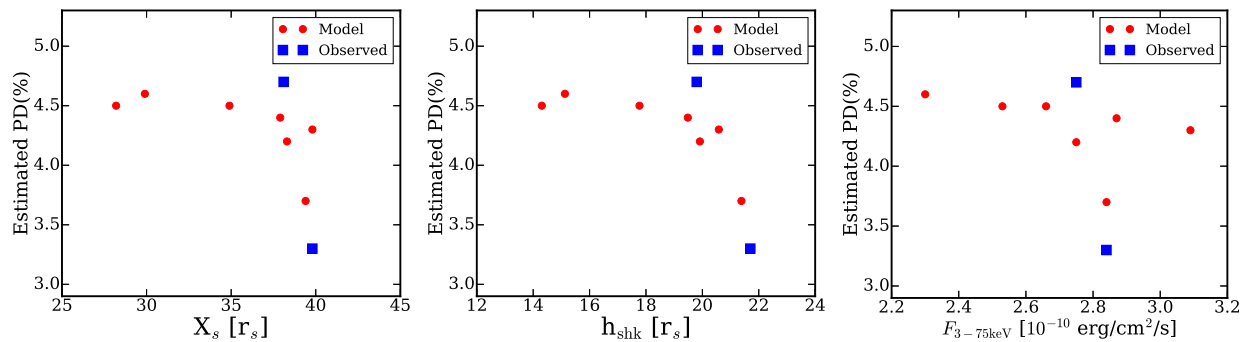


**Figure 3.** Dependence of PD with the geometry of the Comptonizing corona. The left and middle panels show the PD variation with the radial distance and height of the corona, while the right panel shows the PD variation with the observed flux in the 3 – 79 keV band. The red circles show the predicted PD, estimated using spectral model fitted accretion parameters, and the blue squares show the observed upper limit in PD measurement.

research activity. This research used data products provided by the IXPE Team (MSFC, SSC, INAF, and INFN) and distributed with additional software tools by the High-Energy Astrophysics Science Archive Research Center (HEASARC), at NASA Goddard Space Flight Center (GSFC). This research has made use of the *NuSTAR* Data Analysis Software (NuSTARDAS) jointly developed by the ASI Science Data Center (ASDC, Italy) and the California Institute of Technology (Caltech, USA).

**Funding Statement** SM acknowledges Ramanujan Fellowship (# RJF/2020/000113) by SERB-DST, Govt. of India for this research.

**Competing Interests** None

**Data Availability Statement** Data used in this work are publicly available in NASA’s HEASARC archive.

## References

- Arnaud, K. A. 1996. XSPEC: The First Ten Years. In *Astronomical data analysis software and systems v*, edited by George H. Jacoby and Jeannette Barnes, 101:17. Astronomical Society of the Pacific Conference Series.
- Baldini, Luca, Niccolò Bucciantini, Niccolò Di Lalla, Steven Ehlert, Alberto Manfreda, Michela Negro, Nicola Omodei, Melissa Pesce-Rollins, Carmelo Sgrò, and Stefano Silvestri. 2022. ixpeobssim: A simulation and analysis framework for the imaging X-ray polarimetry explorer. *SoftwareX* 19 (July): 101194. <https://doi.org/10.1016/j.softx.2022.101194>. arXiv: 2203.06384 [astro-ph. IM].
- Balestra, I., S. Bianchi, and G. Matt. 2004. The reprocessing features in the X-ray spectrum of the NELG MCG -5-23-16. *A&A* 415 (February): 437–442. <https://doi.org/10.1051/0004-6361:20030211>. arXiv: astro-ph/0311316 [astro-ph].
- Baloković, M., G. Matt, F. A. Harrison, A. Zoghbi, D. R. Ballantyne, S. E. Boggs, F. E. Christensen, et al. 2015. Coronal Properties of the Seyfert 1.9 Galaxy MCG-05-23-016 Determined from Hard X-Ray Spectroscopy with NuSTAR. *ApJ* 800, no. 1 (February): 62. <https://doi.org/10.1088/0004-637X/800/1/62>. arXiv: 1412.5978 [astro-ph. HE].
- Beckmann, V., T. J. -L. Courvoisier, N. Gehrels, P. Lubinski, J. Malzac, P. -O. Petrucci, C. R. Shrader, and S. Soldi. 2008. The efficient low-mass Seyfert MCG-05-23-016. *A&A* 492, no. 1 (December): 93–99. <https://doi.org/10.1051/0004-6361:200810674>. arXiv: 0810.3774 [astro-ph].
- Begelman, M. C., and C. F. McKee. 1983. Compton heated winds and coronae above accretion disks. II. Radiativetransfer and observable consequences. *ApJ* 271 (August): 89–112. <https://doi.org/10.1086/161179>.
- Beheshtipour, Banafsheh, Henric Krawczynski, and Julien Malzac. 2017. The X-Ray Polarization of the Accretion Disk Coronae of Active Galactic Nuclei. *ApJ* 850, no. 1 (November): 14. <https://doi.org/10.3847/1538-4357/aa906a>. arXiv: 1710.00247 [astro-ph. HE].
- Braito, V., J. N. Reeves, G. C. Dewangan, I. George, R. E. Griffiths, A. Markowitz, K. Nandra, et al. 2007. Relativistic Iron K Emission and Absorption in the Seyfert 1.9 Galaxy MCG -5-23-16. *ApJ* 670, no. 2 (December): 978–991. <https://doi.org/10.1086/521916>. arXiv: 0707.2950 [astro-ph].
- Chakrabarti, Sandip, and Lev G. Titarchuk. 1995. Spectral Properties of Accretion Disks around Galactic and Extragalactic Black Holes. *ApJ* 455 (December): 623. <https://doi.org/10.1086/176610>. arXiv: astro-ph/9510005 [astro-ph].
- Chakrabarti, Sandip K. 1999. Estimation and effects of the mass outflow from shock compressed flow around compact objects. *A&A* 351 (November): 185–191. arXiv: astro-ph/9910014 [astro-ph].
- Chatterjee, Rwitika, Vivek K. Agrawal, Kiran M. Jayasurya, and Tilak Katoch. 2023. Spectro-polarimetric view of bright atoll source GX 9+9 using IXPE and AstroSat. *MNRAS* 521, no. 1 (May): L74–L78. <https://doi.org/10.1093/mnras/stad014>. arXiv: 2301.13394 [astro-ph. HE].
- Connors, P. A., T. Piran, and R. F. Stark. 1980. Polarization features of X-ray radiation emitted near black holes. *ApJ* 235 (January): 224–244. <https://doi.org/10.1086/157627>.
- Debnath, D., S. K. Chakrabarti, and S. Mondal. 2014. Implementation of two-component advective flow solution in xspec. *MNRAS* 440 (May): L121–L125. <https://doi.org/10.1093/mnras/slu024>. arXiv: 1402.0989 [astro-ph. HE].
- Dewangan, G. C., R. E. Griffiths, and N. J. Schurch. 2003. XMM-Newton Observations of Broad Iron K $\alpha$  Emission from Seyfert 1.9 Galaxy MCG -5-23-16. *ApJ* 592, no. 1 (July): 52–61. <https://doi.org/10.1086/375640>. arXiv: astro-ph/0304037 [astro-ph].
- Di Marco, Alessandro, Enrico Costa, Fabio Muleri, Paolo Soffitta, Sergio Fabiani, Fabio La Monaca, John Rankin, et al. 2022. A Weighted Analysis to Improve the X-Ray Polarization Sensitivity of the Imaging X-ray Polarimetry Explorer. *AJ* 163, no. 4 (April): 170. <https://doi.org/10.3847/1538-3811/220201093>. arXiv: 2202.01093 [astro-ph. IM].
- Done, Chris, Marek Gierliński, and Aya Kubota. 2007. Modelling the behaviour of accretion flows in X-ray binaries. Everything you always wanted to know about accretion but were afraid to ask. *A&ARv* 15, no. 1 (December): 1–66. <https://doi.org/10.1007/s00159-007-0006-1>. arXiv: 0708.0148 [astro-ph].
- Dovčiak, M., F. Muleri, R. W. Goosmann, V. Karas, and G. Matt. 2008. Thermal disc emission from a rotating black hole: X-ray polarization signatures. *MNRAS* 391, no. 1 (November): 32–38. <https://doi.org/10.1111/j.1365-8950.0809.0418> [astro-ph].

- Gianolli, V. E., D. E. Kim, S. Bianchi, and et al. 2023. Uncovering the geometry of the hot X-ray corona in the Seyfert galaxy NGC 4151 with IXPE. *MNRAS* 523, no. 3 (August): 4468–4476. <https://doi.org/10.1093/mnras/stad607> arXiv: 2303.12541 [astro-ph.GA].
- Haardt, Francesco, and Laura Maraschi. 1993. X-Ray Spectra from Two-Phase Accretion Disks. *ApJ* 413 (August): 507. <https://doi.org/10.1086/173020>.
- Harrison, Fiona A., William W. Craig, Finn E. Christensen, Charles J. Hailey, William W. Zhang, Steven E. Boggs, Daniel Stern, and et al. 2013. The Nuclear Spectroscopic Telescope Array (NuSTAR) High-energy X-Ray Mission. *ApJ* 770, no. 2 (June): 103. <https://doi.org/10.1088/0004-637X/770/2/103> arXiv: 1301.7307 [astro-ph.IM].
- HI4PI Collaboration, N. Ben Bekhti, L. Flöer, R. Keller, J. Kerp, D. Lenz, B. Winkel, et al. 2016. HI4PI: A full-sky H I survey based on EBHIS and GASS. *A&A* 594 (October): A116. <https://doi.org/10.1051/0004-6361/201629178> arXiv: 1610.06175 [astro-ph.GA].
- Ingram, A., M. Ewing, A. Marinucci, and et al. 2023. The X-ray polarization of the Seyfert 1 galaxy IC 4329A. *MNRAS* 525, no. 4 (November): 5437–5449. <https://doi.org/10.1093/mnras/stad2625> arXiv: 2305.13028 [astro-ph.HE].
- Iyer, N., A. Nandi, and S. Mandal. 2015. Determination of the Mass of IGR J17091–3624 from “Spectro-temporal” Variations during the Onset Phase of the 2011 Outburst. *ApJ* 807, no. 1 (July): 108. <https://doi.org/10.1088/0004-637X/807/1/108> arXiv: 1505.02529 [astro-ph.HE].
- Jayasurya, Kiran M., Vivek K. Agrawal, and Rwitika Chatterjee. 2023. Detection of significant X-ray polarization from transient NS-LMXB XTE J1701–462 with IXPE and its implication on the coronal geometry. *MNRAS* 525, no. 3 (November): 4657–4662. <https://doi.org/10.1093/mnras/stad2604> arXiv: 2302.03396 [astro-ph.HE].
- Joye, W. A., and E. Mandel. 2003. New Features of SAOImage DS9. In *Astronomical data analysis software and systems xii*, edited by H. E. Payne, R. I. Jedrzejewski, and R. N. Hook, 295:489. Astronomical Society of the Pacific Conference Series. January.
- Kalberla, P. M. W., W. B. Burton, Dap Hartmann, E. M. Arnal, E. Bajaja, R. Morras, and W. G. L. Pöppel. 2005. The Leiden/Argentine/Bonn (LAB) Survey of Galactic HI. Final data release of the combined LDS and IAR surveys with improved stray-radiation corrections. *A&A* 440, no. 2 (September): 775–782. <https://doi.org/10.1051/0004-6361:20041864> arXiv: astro-ph/0504140 [astro-ph].
- Kislat, F., B. Clark, M. Beilicke, and H. Krawczynski. 2015. Analyzing the data from X-ray polarimeters with Stokes parameters. *Astroparticle Physics* 68 (August): 45–51. <https://doi.org/10.1016/j.astropartphys.2015.02.007> arXiv: 1409.6214 [astro-ph.IM].
- Li, Li-Xin, Ramesh Narayan, and Jeffrey E. McClintock. 2009. Inferring the Inclination of a Black Hole Accretion Disk from Observations of its Polarized Continuum Radiation. *ApJ* 691, no. 1 (January): 847–865. <https://doi.org/10.1088/0004-637X/691/1/847> arXiv: 0809.0866 [astro-ph].
- Liu, Victor, Abderahmen Zoghbi, and Jon M. Miller. 2023. Detection of Asymmetry in the Narrow Fe K $\alpha$  Emission Line in MCG-5-23-16 with Chandra. *arXiv e-prints* (December): arXiv:2312.16354. <https://doi.org/10.48550/arXiv.2312.16354> arXiv: 2312.16354 [astro-ph.HE].
- Marinucci, A., F. Muleri, M. Dovciak, S. Bianchi, F. Marin, G. Matt, F. Ursini, et al. 2022. Polarization constraints on the X-ray corona in Seyfert Galaxies: MCG-05-23-16. *MNRAS* 516, no. 4 (November): 5907–5913. <https://doi.org/10.1093/mnras/stac2634> arXiv: 2207.09338 [astro-ph.HE].
- Mattson, B. J., and K. A. Weaver. 2004. RXTE and BeppoSAX Observations of MCG -5-23-16: Reflection from Distant Cold Material. *ApJ* 601, no. 2 (February): 771–777. <https://doi.org/10.1086/380502> arXiv: astro-ph/0310468 [astro-ph].
- Molina, M., L. Bassani, A. Malizia, J. B. Stephen, A. J. Bird, A. Bazzano, and P. Ubertini. 2013. Hard-X-ray spectra of active galactic nuclei in the INTEGRAL complete sample. *MNRAS* 433, no. 2 (August): 1687–1700. <https://doi.org/10.1093/mnras/stt844> arXiv: 1305.2722 [astro-ph.HE].
- Mondal, Santanu, and Sandip K. Chakrabarti. 2013. Spectral properties of two-component advective flows with standing shocks in the presence of Comptonization. *MNRAS* 431, no. 3 (May): 2716–2722. <https://doi.org/10.1093/mnras/stt1403>.
- . 2021. Spectral signature of mass outflow in the two component advective flow paradigm. *The Astrophysical Journal* 920, no. 1 (October): 41. <https://doi.org/10.3847/1538-4357/ac14c2> <https://doi.org/10.3847/1538-4357/abf077>.
- Mondal, Santanu, Sandip K. Chakrabarti, and Dipak Debnath. 2014. Spectral signatures of dissipative standing shocks and mass outflow in presence of Comptonization around a black hole. *Ap&SS* 353, no. 1 (September): 221–231. <https://doi.org/10.1007/s10509-014-2008-6> arXiv: 1406.1878 [astro-ph.HE].
- Onori, F., F. Ricci, F. La Franca, S. Bianchi, A. Bongiorno, M. Brusa, F. Fiore, et al. 2017. Detection of faint broad emission lines in type 2 AGN – II. On the measurement of the black hole mass of type 2 AGN and the unified model. *MNRAS* 468, no. 1 (June): L97–L102. <https://doi.org/10.1093/mnras/stx1403> arXiv: 1703.05167 [astro-ph.GA].
- Pal, Indrani, C. S. Stalin, Rwitika Chatterjee, and Vivek K. Agrawal. 2023. X-ray polarization observations of IC 4329A with IXPE: Constraining the geometry of X-ray corona. *Journal of Astrophysics and Astronomy* 44, no. 2 (December): 87. <https://doi.org/10.1007/s12036-023-09981-5> arXiv: 2305.09365 [astro-ph.HE].
- Papadakis, S. Bianchi, M. Guainazzi, G. Matt, P. Uttley, and N. F. Bonilla. 2012. CAIXA: a catalogue of AGN in the XMM-Newton archive. III. Excess variance analysis. *A&A* 542 (June): A83. <https://doi.org/10.1051/0004-6361/1112.2744> arXiv: 1112.2744 [astro-ph.HE].
- Reeves, James N., Hisamitsu Awaki, Gulab C. Dewangan, Andy C. Fabian, Masushi Fukazawa, Luigi Gallo, Richard Griffiths, et al. 2007. Revealing the High Energy Emission from the Obscured Seyfert Galaxy MCG-5-23-16 with Suzaku. *PASJ* 59 (January): 301–314. <https://doi.org/10.1093/pasj/59.sp1> arXiv: astro-ph/0610434 [astro-ph].
- Schnittman, Jeremy D., and Julian H. Krolik. 2010. X-ray Polarization from Accreting Black Holes: Coronal Emission. *ApJ* 712, no. 2 (April): 908–924. <https://doi.org/10.1088/0004-637X/712/2/908> arXiv: 0912.0907 [astro-ph.HE].
- Serafinelli, Roberto, Andrea Marinucci, Alessandra De Rosa, Stefano Bianchi, Riccardo Middei, Giorgio Matt, James N. Reeves, et al. 2023. A remarkably stable accretion disc in the Seyfert galaxy MCG-5-23-16. *MNRAS* 526, no. 3 (December): 3540–3547. <https://doi.org/10.1093/mnras/stad2801> arXiv: 2309.06092 [astro-ph.HE].
- Sunyaev, R. A., and L. G. Titarchuk. 1980. Comptonization of X-rays in plasma clouds. Typical radiation spectra. *A&A* 500 (June): 167–184.
- . 1985. Comptonization of low-frequency radiation in accretion disks. Angular distribution and polarization of hard radiation. *A&A* 143, no. 2 (February): 374–388.
- Tagliacozzo, D., A. Marinucci, F. Ursini, G. Matt, S. Bianchi, L. Baldini, T. Barnouin, N. Caverro Rodriguez, A. De Rosa, and et al. 2023. The geometry of the hot corona in MCG-05-23-16 constrained by X-ray polarimetry. *MNRAS* 525, no. 3 (November): 4735–4743. <https://doi.org/10.1093/mnras/stad2604> arXiv: 2305.10213 [astro-ph.HE].
- Tamborra, Francesco, Giorgio Matt, Stefano Bianchi, and Michal Dovciak. 2018. MoCA: A Monte Carlo code for Comptonisation in Astrophysics. I. Description of the code and first results. *A&A* 619 (November): A105. <https://doi.org/10.1051/0004-6361/201732023> arXiv: 1808.07399 [astro-ph.HE].
- Veron, P., P. O. Lindblad, E. J. Zuiderwijk, M. P. Veron, and G. Adam. 1980. On the nature of the so-called narrow-line X-ray galaxies. *A&A* 87, nos. 1–2 (July): 245–249.
- Wang, Yu, M. Ghasemi-Nodehi, Matteo Guainazzi, and Cosimo Bambi. 2017. The Spin of the Supermassive Black Hole in MCG-05-23-16. *arXiv e-prints* (March): arXiv:1703.07182. <https://doi.org/10.48550/arXiv.1703.07182> arXiv: 1703.07182 [astro-ph.HE].
- Weaver, K. A., T. Yaqoob, R. F. Mushotzky, J. Nousek, I. Hayashi, and K. Koyama. 1997. Iron K $\alpha$  Evidence for Two X-Ray Reproprocessors in MCG -5-23-16. *ApJ* 474, no. 2 (January): 675–685. <https://doi.org/10.1086/303488>.

- Wegner, G., M. Bernardi, C. N. A. Willmer, L. N. da Costa, M. V. Alonso, P. S. Pellegrini, M. A. G. Maia, O. L. Chaves, and C. Rit . 2003. Redshift-Distance Survey of Early-Type Galaxies: Spectroscopic Data. *AJ* 126, no. 5 (November): 2268–2280. <https://doi.org/10.1086/378959>. arXiv: astro-ph/0308357 [astro-ph].
- Weisskopf, Martin C., Brian Ramsey, Stephen O’Dell, Allyn Tennant, Ronald Elsner, Paolo Soffitta, Ronaldo Bellazzini, et al. 2016. The Imaging X-ray Polarimetry Explorer (IXPE). In *Space telescopes and instrumentation 2016: ultraviolet to gamma ray*, edited by Jan-Willem A. den Herder, Tadayuki Takahashi, and Marshall Bautz, 9905:990517. Society of Photo-Optical Instrumentation Engineers (SPIE) Conference Series. July. <https://doi.org/10.1117/12.2235240>.
- Wilms, J., A. Allen, and R. McCray. 2000. On the Absorption of X-Rays in the Interstellar Medium. *ApJ* 542, no. 2 (October): 914–924. <https://doi.org/10.1086/317016>. arXiv: astro-ph/0008425 [astro-ph].
- Zoghbi, Abderahmen, G. Matt, J. M. Miller, A. M. Lohfink, D. J. Walton, D. R. Ballantyne, J. A. Garc a, et al. 2017. A Long Look at MCG-5-23-16 with NuSTAR. I. Relativistic Reflection and Coronal Properties. *ApJ* 836, no. 1 (February): 2. <https://doi.org/10.3847/1538-4357/aa582c>. arXiv: 1701.02309 [astro-ph.HE].